

## Local predictability and nonhyperbolicity through finite Lyapunov exponent distributions in two-degrees-of-freedom Hamiltonian systems

Juan C. Vallejo

*Nonlinear Dynamics, Chaos and Complex Systems Group, Departamento de Física, Universidad Rey Juan Carlos, Tulipán s/n, 28933 Móstoles, Madrid, Spain*

Ricardo L. Viana

*Departamento de Física, Universidade Federal do Paraná, C. P. 190 81, 81531-990, Curitiba, Paraná, Brazil*

Miguel A. F. Sanjuán

*Nonlinear Dynamics, Chaos and Complex Systems Group, Departamento de Física, Universidad Rey Juan Carlos, Tulipán s/n, 28933 Móstoles, Madrid, Spain*

(Received 13 September 2007; revised manuscript received 5 November 2008; published 4 December 2008)

By using finite Lyapunov exponent distributions, we get insight into both the local and global properties of a dynamical flow, including its nonhyperbolic behavior. Several distributions of finite Lyapunov exponents have been computed in two prototypical four-dimensional phase-space Hamiltonian systems. They have been computed calculating the growth rates of a set of orthogonal axes arbitrarily pointed at given intervals. We analyze how such distributions serve or not for tracing the orbit nature and local flow properties such as the unstable dimension variability, as the axes are allowed or not to tend to the largest stretching direction. The relationship between the largest and closest to zero exponent distribution is analyzed. It shows a linear dependency at short intervals, related to the number of degrees of freedom of the system. Finally, the hyperbolicity indexes, associated to the shadowing times, are calculated. They provide interesting information at very local scales, even when there are no Gaussian distributions and the values cannot be regarded as random variables.

DOI: [10.1103/PhysRevE.78.066204](https://doi.org/10.1103/PhysRevE.78.066204)

PACS number(s): 05.45.-a

### I. INTRODUCTION

Understanding the dynamics of realistic conservative systems, is a fundamental issue in nonlinear dynamics and statistical physics, with direct applications in many fields such as astronomy, plasma physics, and atomic physics [1]. But the dynamical analysis of Hamiltonian flows with more than two-dimensional phase spaces, has some important issues to take into account. The first, not as trivial as one might think, is the visualization of the orbits and the selection of a proper surface of section. Another one is the increase of complexity of the algorithms for searching periodic orbits, which must deal with additional constraints when the energy is a conserved quantity. Searching engines based in Newton algorithms must explore the phase space keeping in the same initial energy subspace.

The search for invariants is one of the most common tools for understanding the dynamics of nonintegrable systems (see a classical example in [2]). Usually, the fixed points and associated periodic orbits, being the basic building blocks of the dynamics, are located and studied. Later on, the surroundings are analyzed, as the stable orbits are mostly surrounded by quasiperiodic orbits, while unstable periodic orbits by chaotic ones. But the complexity of the higher-order orbits makes this procedure less straightforward. The computation of the invariant tori and invariant manifolds also gain a high degree of complexity in realistic models.

An alternative approach is to characterize the instability by using numerical indicators such as the Lyapunov exponents. Due to the sometimes slow convergence of the asymptotic value, many studies have used faster convergence

indexes such as the rotation index [3], the smaller alignment index [4], the mean exponential growth factor of nearby orbits [5] or the fast lyapunov indicator [6].

These indicators allow for distinguishing among the ordered, chaotic or weak chaotic orbits, and even among the resonant and nonresonant regions [7]. However, Lyapunov exponents still remain valid indicators since they are quite easy to compute numerically, and they do not depend upon the metric. More importantly, in addition to mapping the global degree of instability of a system, they can also reflect the local properties of the flow when computed during very short intervals including the sticky behavior of chaotic orbits near remnants of periodic orbits embedded in the chaotic sea.

Our work focuses on analyzing some prototypical orbits in a four-dimensional phase-space Hamiltonian flow (two-degrees-of-freedom flow), by means of finite Lyapunov exponent distributions. Most studies are devoted to the characterization of a system using only the first (largest) Lyapunov exponent. But the following finite exponents and their correlations also provide interesting information. We will focus on their distributions formed when the axes of one ellipse generated along an orbit are allowed or not to tend to the largest stretching direction before being reoriented after a given interval. We will see how they may reflect the unstable dimension variability property, which has direct consequences in the predictability of the orbit. We will compute as well the hyperbolicity indexes associated to every exponent to analyze the shadowing times, which define the duration over which there exists a model trajectory consistent with the real system.

The rest of the paper is organized as follows. Section II reviews some basic concepts and definitions for Lyapunov

exponents. Section III does the same for the finite Lyapunov exponent distributions. A description of the model we treat in this paper as well as the numerical method of integration is contained in Sec. IV. The distributions of the exponents are found in Sec. V. The relation between the first (largest) and second finite exponents is treated in Sec. VI. In Sec. VII we discuss the breakdown of hyperbolicity due to unstable dimension variability, the shadowing properties, and the relationship with the calculated distributions. Finally, Sec. VIII is devoted to our conclusions.

## II. LYAPUNOV EXPONENTS

The ordinary (also named global or infinite) Lyapunov exponent describes the evolution in time of the distance  $z(t)$  between two nearby initial conditions, separated  $\delta z(0)$  at  $t=0$ , and it is defined in the following manner:

$$\lambda = \lim_{t \rightarrow \infty} \lim_{\delta z(0) \rightarrow 0} \frac{1}{t} \ln \frac{\delta z(t)}{\delta z(0)}. \quad (1)$$

In Hamiltonian systems, because of their symplectic nature,  $\lambda_i = -\lambda_{5-i}$  for  $i=1, \dots, 4$  and only two of the different values of  $\lambda$  are independent. The second exponent has a zero value in the limiting case, as is tangent to the trajectory, and there is never any divergence for a perturbed trajectory in the direction of the unperturbed trajectory.

The analysis of the nontrivial exponent values provide valuable information, such as the presence of new isolating integrals. If the first is zero, the motion is integrable. If it is nonzero and positive, there is an exponential separation of trajectories.

In practice, all numerically computed exponents, or those from experimental data, are computed over finite-time intervals. Such values are generically named as finite Lyapunov exponents. Unlike the ordinary Lyapunov exponents, which take the same values for almost every initial condition in every region if chaoticity is sufficiently strong (except for a Lebesgue measure zero set, following Oseledec theorem), the values of the exponents over finite times are generally different and may change in sign along one orbit.

Depending on the precise definitions, among others, we can cite the finite-size Lyapunov exponents [8] or the generalized Lyapunov exponents [9]. For our purposes, we will focus on the following definition:

$$\chi(\Delta t) = \frac{1}{\Delta t} \lim_{\delta z(0) \rightarrow 0} \ln \frac{\delta z(\Delta t)}{\delta z(0)}, \quad (2)$$

which is derived from the Eq. (1) for finite averaging times. This is named as effective Lyapunov exponent for large but finite intervals [10], meanwhile the term local Lyapunov exponent is preferred when such interval is small enough. The term transient Lyapunov exponent is found in [11], meaning intervals not large enough to ensure a satisfactory reduction of the fluctuations but small enough to reveal slow trends. Typical options for  $\Delta t$  are  $T_{\text{cross}}$ , the crossing time of the Poincaré surface of section,  $T_{\text{dyn}}$ , the dynamical time of the system, or any other physically meaningful time scale.

One standard technique for exponent computation consists of integrating two nearby trajectories  $z(t)$  and  $z'(t)$  with

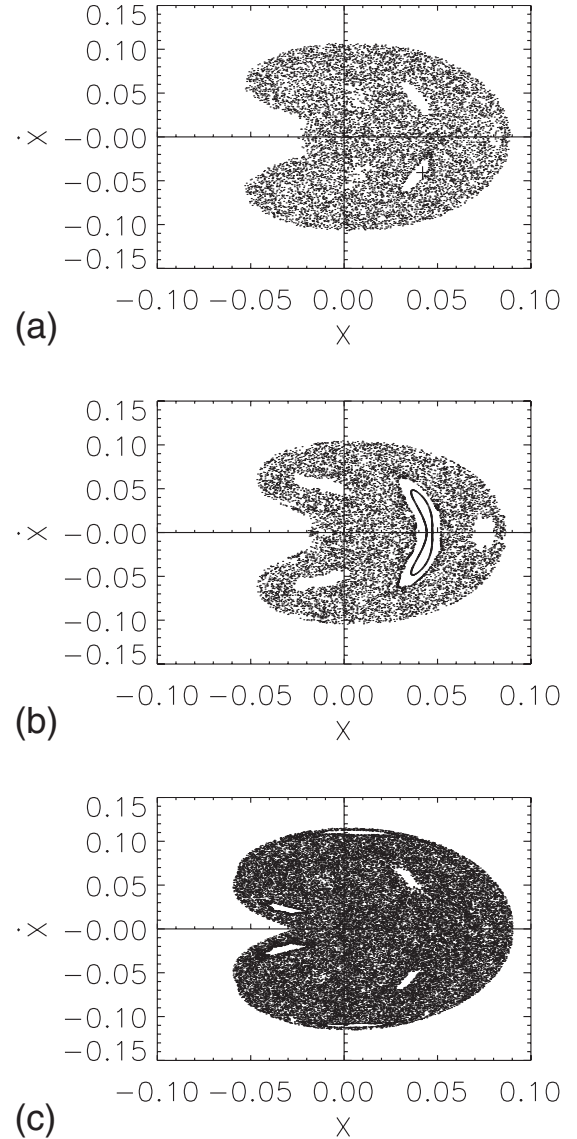


FIG. 1. Poincaré cross sections with the  $y=0$  plane for the studied Hamiltonian and three values of the  $\epsilon$  parameter. Initial condition is  $x=0.03744$ ,  $y=0$ ,  $\dot{x}=0.0480$ . (a)  $\epsilon=4.5$ , period-2 orbit (marked with a cross). (b)  $\epsilon=4.4$ , between tori orbit (big lobe). (c)  $\epsilon=4.6$ , chaotic orbit (full filling the phase space). The cross section of another ergodic orbit ( $x=0.03$ ,  $y=0$ ,  $\dot{x}=0.04796$ ) has been also plotted in the first and second cases in order to ease the visualization of the phase portrait.

initial Euclidean distance  $\delta z(0)=\delta$  until their separation becomes larger at time  $T_r$  than  $r\delta$ , being  $r$  a given constant coefficient. The perturbed trajectory  $z'(T_r)$  is then rescaled at the original distance  $\delta$ , keeping the direction  $z'-z$  constant.

We get different growth rates not only depending on the initial condition, but also on the initial orientation of the perturbation [12]. The finite-time Lyapunov exponent refers to when the direction coincides with the direction which will have grown the most under the linearized dynamics, the right singular vector of the Jacobian of the flow. The finite-sample Lyapunov exponents are defined when the direction points towards the local orientation of the globally fastest growing

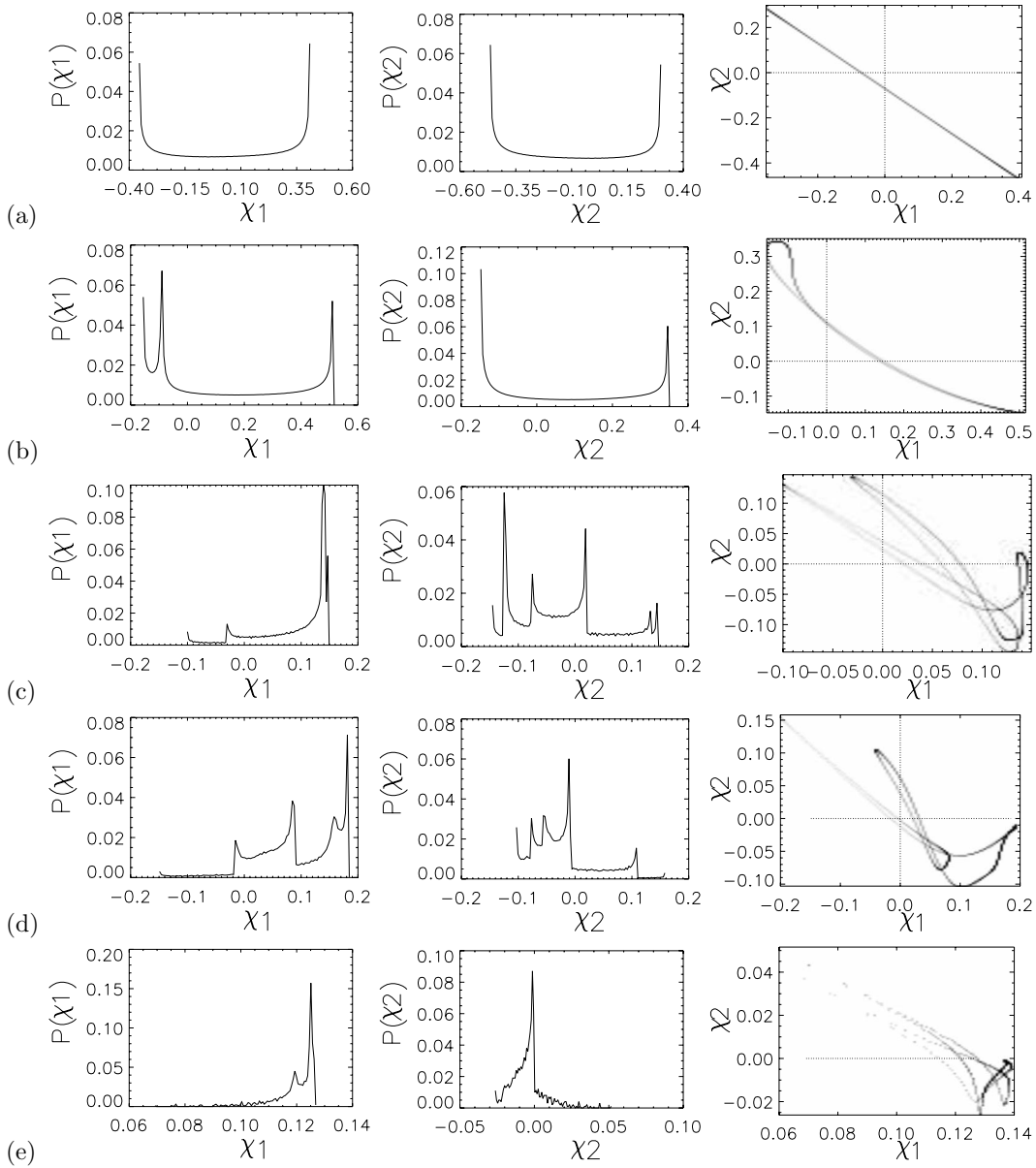


FIG. 2. Finite Lyapunov exponent distributions for the Eq. (3) Hamiltonian and  $\epsilon=4.5$ , 2-periodic orbit. (a)  $\Delta t=0.01$ , (b)  $\Delta t=1$ , (c)  $\Delta t=7$ , (d)  $\Delta t=10$ , (e)  $\Delta t=100$ .

direction, and are found to be smaller than the former definition.

There are several other methods for computing the exponents, each one possessing advantages and disadvantages (see Ref. [13] for a comparison). We will concentrate on the well-known method proposed by Ref. [14]. The global exponents are derived from the growth rate of the axes of one ellipse centered in the initial position. The calculation is started with an arbitrary set of orthogonal unit vectors. After a few steps, the initial vectors tend to align with the eigenvectors corresponding to the dominant exponents. The Jacobian components will be the new orthogonal axes, defining the evolved ellipsoid. Their multiplicative growth rates define the Lyapunov numbers.

As initial arbitrary set, we could use the eigenvectors of the Jacobian matrix, and compute the exponents from the

associated eigenvalues. These finite-time exponents can trace the stable and unstable manifolds (the latter with a time backwards integration) [15,16]. Note that in turn, the angle of both manifolds provides the nonhyperbolic nature of the system. But in which concerns this paper, the ellipse axes will be initialized with no particular direction (i.e., not pointing to the Jacobian eigenvectors). We aim to see how even in this case and with the shortest intervals, the shapes of the distribution of values along a given orbit, chaotic or not, still reflect in detail the local flow of the system.

### III. FINITE LYAPUNOV EXPONENT DISTRIBUTIONS

If we make a partition of the whole integration time along one orbit into a series of time intervals of size  $\Delta t$ , then it is possible to compute the finite time Lyapunov exponent  $\chi(\Delta t)$

TABLE I. Numerical indexes associated to the finite Lyapunov exponent distributions corresponding to Eq. (3), case  $\epsilon=4.5$ , period-2 orbit, for several  $\Delta t$  sizes. ( $\sigma$  is the standard deviation,  $k$  the kurtosis,  $F_+$  the probability of positivity,  $h$  the hyperbolicity index.)

$\Delta t$	Mean	Median	$\sigma$	k	$F_+$	$h$
			$\chi_1$			
0.01	0.048	0.065	0.27	-1.45	0.55	1.35
0.1	0.048	0.067	0.29	-1.45	0.55	1.19
1	0.14	0.070	0.24	-1.46	0.56	4.65
7	0.092	0.12	0.066	0.36	0.86	42.45
10	0.095	0.091	0.072	0.014	0.89	37.22
100	0.12	0.12	0.0084	11.32	1.00	3406.33
			$\chi_2$			
0.01	-0.096	-0.11	0.27	-1.45	0.39	2.69
0.1	-0.076	-0.095	0.28	-1.44	0.42	1.87
1	0.082	0.063	0.18	-1.55	0.56	4.77
7	-0.021	-0.028	0.080	-0.74	0.38	6.66
10	-0.02	-0.031	0.057	0.38	0.22	12.70
100	-0.0041	-0.0038	0.011	4.77	0.19	68.54

for each interval. When such distribution is normalized, dividing it by the total number of intervals, we obtain a density function  $P(\chi)$  that gives the probability of getting a given value  $\chi$  between  $[\chi, \chi+d\chi]$ .

We can get information about the degree of instability of the orbit by subtracting different spectra [17], by deriving their power spectrum via the Fourier transform [18], or by analyzing their shapes and cumulants or  $q$  moments of the distribution.

The distributions of effective Lyapunov exponents can be studied from the cumulant generating function, defined as the logarithm of the moment generating function, which is itself the Fourier transform of the probability density function [10]. The first four cumulants are the mean, variance, skewness, and kurtosis of the distributions. As they reflect the deviation from Gaussianity, they reflect the deviation from the fully chaotic case. The generalized exponents are associated to the order- $q$  moments of the distributions [9,19].

For some maps, like the Ulam map  $x \mapsto 4x(1-x)$ , explicit analytical expressions can be found for such probability exponents. In such cases, the probability distributions of time- $n$  exponents strongly deviate from the Gaussian shape, decaying with exponential tails and presenting  $2^{n-1}$  spikes that narrow and accumulate close to the mean value with increasing  $n$  [20]. Such tails and spikes were described for the Hénon-Heiles system in [21].

Two ways are possible for numerically calculating the distributions. We can derive the distribution values from an ensemble of initial conditions located in the same dynamical domain or from an ensemble of initial conditions resulting from one single orbit integration. Only when the phase space is largely stochastic and the regular regions small, the results from both methods coincide, in agreement with the ergodic theorem. As we aim to use the distributions for characterizing different orbital behaviors, we have taken the second procedure, meaning that once started the integration, after a

$\Delta t$  interval, the growth rates are saved and the ellipsoid axes are reset again to point to arbitrary directions.

#### IV. DESCRIPTION OF THE MODEL AND INTEGRATOR

We have studied the four-dimensional phase-space Hamiltonian, two-degrees-of-freedom, originally studied by Contopoulos in Ref. [22], and given by

$$H = \frac{1}{2}(p_x^2 + p_y^2) + \frac{1}{2}(Ax^2 + By^2) - \epsilon xy^2. \quad (3)$$

This model represents two nonlinearly coupled oscillators. We have chosen it because in spite of its simplicity, it provides a rich dynamical behavior.

In addition, it is a physically meaningful flow. The origins of this model are traced to the galactic dynamics field. It belongs to the so-called galactic-type potentials [23]. These systems are reduced potentials on the meridian plane  $V(r, z)$  of an axisymmetric galaxy, where the equilibrium point  $x=y=0$  represents a stable circular orbit. Their best-known member is the Hénon-Heiles system. We already studied the local instability in this system through the finite-time Lyapunov exponents in [21], and now we extend these previous results to the Hamiltonian given by Eq. (3).

The Hénon-Heiles system was one of the first examples used to show how very simple systems possess highly complicated dynamics. It contains two, properly weighted, coupling terms,  $x^2y$  and  $y^3$ , leading to a Hamiltonian with a  $2\pi/3$  rotation symmetry and three exits in the potential well. The model given by Eq. (3) can be seen as a simpler version. This model has only one mixed higher-order term,  $xy^2$ , which introduces the essential nonlinearity of the problem, has  $y$ -axis symmetry and only two exits.

The amplitude parameters are  $A=1.6$  and  $B=0.9$ . Such values are chosen to be near the resonance  $\sqrt{A/B}=4/3$  [22]. The sampled initial condition is  $x=0.03744$ ,  $y=0$ ,  $\dot{x}$

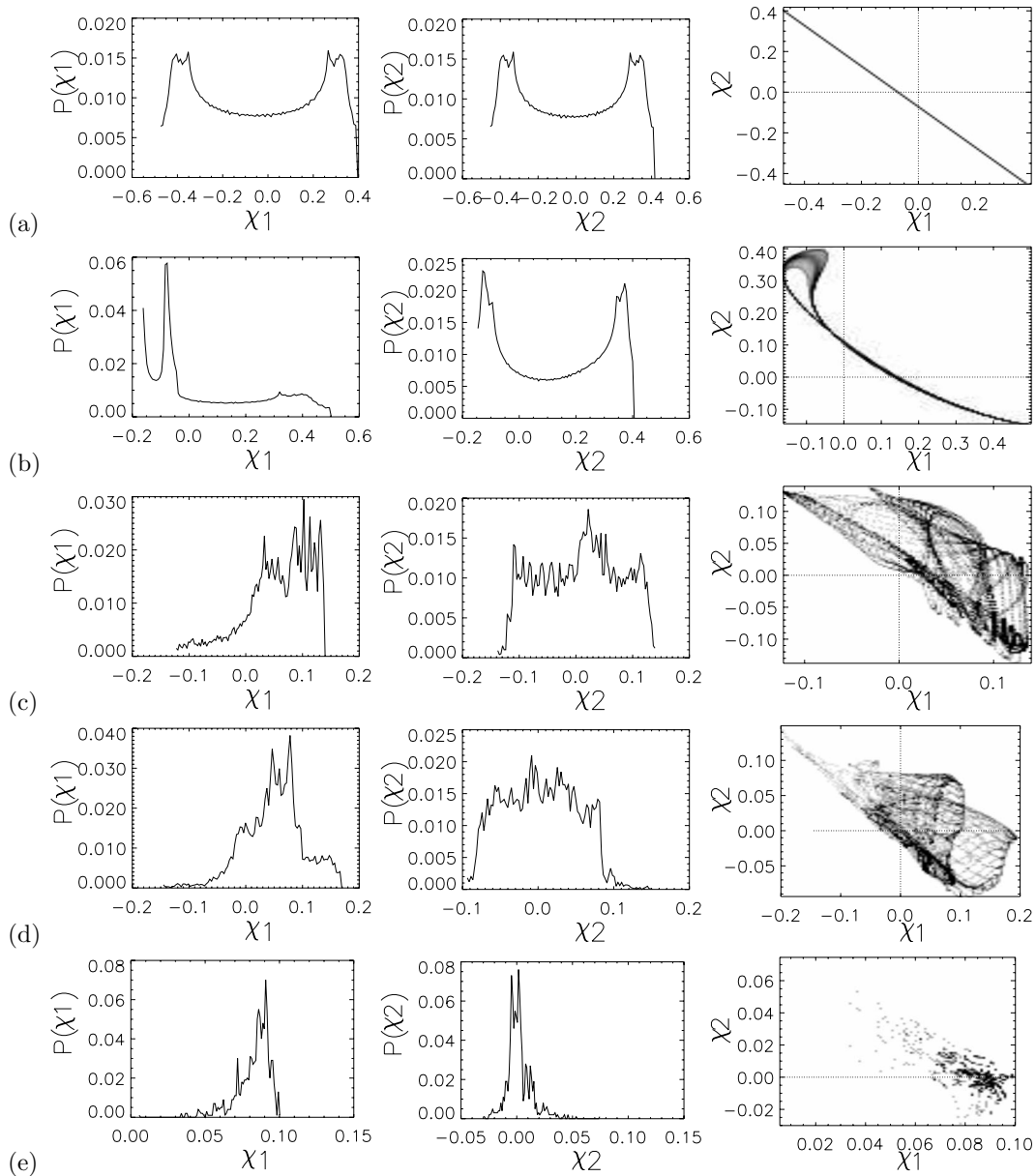


FIG. 3. Finite Lyapunov exponent distributions for the Eq. (3) Hamiltonian and  $\epsilon=4.4$ , between tori orbit. (a)  $\Delta t=0.01$ , (b)  $\Delta t=1$ , (c)  $\Delta t=7$ , (d)  $\Delta t=10$ , (e)  $\Delta t=100$ .

$=0.0480$ , associated to the regular motion of Ref. [24]. For this initial condition, depending on the value of the coupling parameter  $\epsilon$ , different orbit types are found. We have selected three values of  $\epsilon$ , namely, 4.4, 4.5, and 4.6. The energy value is set to  $E=0.00765$ , which in the third case is close to the escape energy, given by  $E_{\text{escape}} = \frac{1}{8} \frac{AB^2}{\epsilon^2}$ .

We have used a Runge-Kutta integrator of fourth order with time step equal to 0.01. A sixth order leads to the same results. Note that such a standard integrator may be thought as quantitatively accurate, but not qualitatively, as small errors may not conserve the energy, contrary to a symplectic scheme. But even when symplectic schemes have generally a better performance in long-term integrations, standard Runge-Kutta is simple and fast. The energy value was checked at each step in order to verify that it keeps constant throughout the computation, as well as the relevant

Lyapunov exponents pairing consequence of the Hamiltonian nature. Indeed, selecting a given symplectic scheme is not as straightforward as one may think. Energy conservation is not always the invariant that must be preserved (it may be the angular momentum first integral), and integrable Hamiltonians approximated by symplectic schemes may manifest apparent chaos [25]. Indeed, the only integrator which preserves all invariants has been proved to be the true solution itself (see a review on the subject in [26]).

## V. FINITE-EXPONENT-DISTRIBUTION COMPUTATIONS

There are several studies which model universal features of the Lyapunov spectra based on the properties of an infinite set of matrices [27]. The effective Lyapunov exponents as logarithms of products of  $n$  matrices behave essentially like

TABLE II. Numerical indexes associated to the finite Lyapunov exponent distributions corresponding to Eq. (3), case  $\epsilon=4.4$ , between tori orbit, for several  $\Delta t$  sizes. ( $\sigma$  is the standard deviation,  $k$  the kurtosis,  $F_+$  the probability of positivity,  $h$  the hyperbolicity index.)

$\Delta t$	Mean	Median	$\sigma$	k	$F_+$	$h$
			$\chi_1$			
0.01	-0.034	-0.033	0.27	-1.42	0.46	0.92
0.1	-0.039	-0.038	0.29	-1.42	0.46	0.93
1	0.077	-0.022	0.20	-1.11	0.47	3.78
7	0.060	0.070	0.059	0.34	0.85	34.88
10	0.054	0.056	0.052	0.48	0.84	40.03
100	0.083	0.086	0.010	4.51	0.99	1472.67
			$\chi_2$			
0.01	-0.013	-0.014	0.27	-1.42	0.48	0.37
0.1	0.012	-0.0094	0.288	-1.42	0.50	0.29
1	0.13	0.14	0.19	-1.53	0.65	7.58
7	0.0091	0.014	0.071	-1.07	0.55	3.66
10	0.0053	0.0049	0.048	-0.91	0.52	4.54
100	0.0023	0.0010	0.0010	4.69	0.50	46.74

averages of  $n$  random variables. Over short times, they are correlated, leading to a linear dependency of the cumulant generating function with  $n$  [10]. Over long times, correlations may be lost. But with intermittency or in area preserving maps, there are still long-time correlations, different scaling properties, and multifractal structure with the sampling interval  $\Delta t$ . We cite among others some general results in [28,29] or [30], some numerical findings in [31] or [21], and specifically, one Hamiltonian map scaling behavior in [32].

We focus here on comparing, for different orbits types, the distributions generated when the axes of the ellipse centered in the initial condition are allowed or not to tend to the largest stretching direction before being repointed after  $\Delta t$  time units. This section describes how these distributions still provide information about the different dynamics.

**A. Periodic orbit,  $\epsilon=4.5$**

The first orbit is a period-2 orbit with Poincaré crossing time  $T_{\text{cross}} \sim 7.3$ , which appears in Fig. 1(a) as a cross symbol. The density functions for the first and the second Lyapunov exponents are plotted in Fig. 2, and their numerical characterization is found in Table I.

The distribution computed with the shortest possible interval  $\Delta t=0.01$ , the integration step, appears in Fig. 2, panel (a). Its shows the typical shape associated to a periodic orbit. For an interval 10 times larger,  $\Delta t=0.1$  (interval still below  $T_{\text{cross}}$ ), the figures are nearly identical to the previous ones, thus they are not drawn. The fact of both being equal is not evident, as the local ellipsoid axes have now evolved a few steps, having the possibility of relaxing in the direction that permits the largest stretching, and pointing to the direction of fastest separation.

For  $\Delta t=1$ , panel (b), a new peak appears in the distribution of the largest exponent  $\chi_1$ , but the  $\chi_2$  distribution remains the same. This means different rates in the evolution

towards the invariant measure. When  $\Delta t \sim T_{\text{cross}}$ , panel (c), the  $\chi_1$  distributions jump towards the positive values.

This leads to think of  $T_{\text{cross}}$  as a threshold separating different regimes in the distributions, tracing local and nonlocal behavior. Even when the choice of the Poincaré section is somehow arbitrary, it is based in the symmetry  $y=0$  of the potential, thus it makes sense that the crossing time for closing an orbit (if periodic) will lead to such a threshold.

At larger intervals,  $\Delta t=10$ , panel (d), the oscillations around zero begin to be lost. Finally, with  $\Delta t=100$ , panel (e), we are integrating several  $T_{\text{cross}}$  cycles, and the distributions resemble peaks centered around the  $\lambda_1 \sim 0.0125$  and  $\lambda_2 \sim 0$  asymptotic Lyapunov values.

**B. Chaos between two KAM tori,  $\epsilon=4.4$**

Quasiperiodic orbits are characterized by a linear divergence of neighboring trajectories, all asymptotic exponents are zero and the motion is confined within a torus. With  $\epsilon=4.4$ , the initial condition is interesting, as it does not lead to a quasiperiodic motion but to a trajectory running on a very small chaos strip between two invariant tori. The Poincaré cross section of this orbit appears as an elongated lobe in Fig. 1(b). The density functions for the first and the second Lyapunov exponents are plotted in Fig. 3. The numerical indexes which characterize such distributions are found in Table II.

The main time scale to take into account seems to be again the crossing time,  $T_{\text{cross}} \sim 7$ . There is another physically meaningful time scale, which is the period to roughly cover the whole Poincaré cross section,  $T_{\text{lobe}} \sim 136$ .

For the shortest interval sizes,  $\Delta t=0.01$ , panel (a), and  $\Delta t=0.1$ , not shown, the distributions are similar, roughly double peaked, reflecting the confined motion. When the interval is increased up to  $\Delta t=1$ , panel (b), there is a change in shape for  $\chi_1$ , with a morphology no longer similar to a peri-

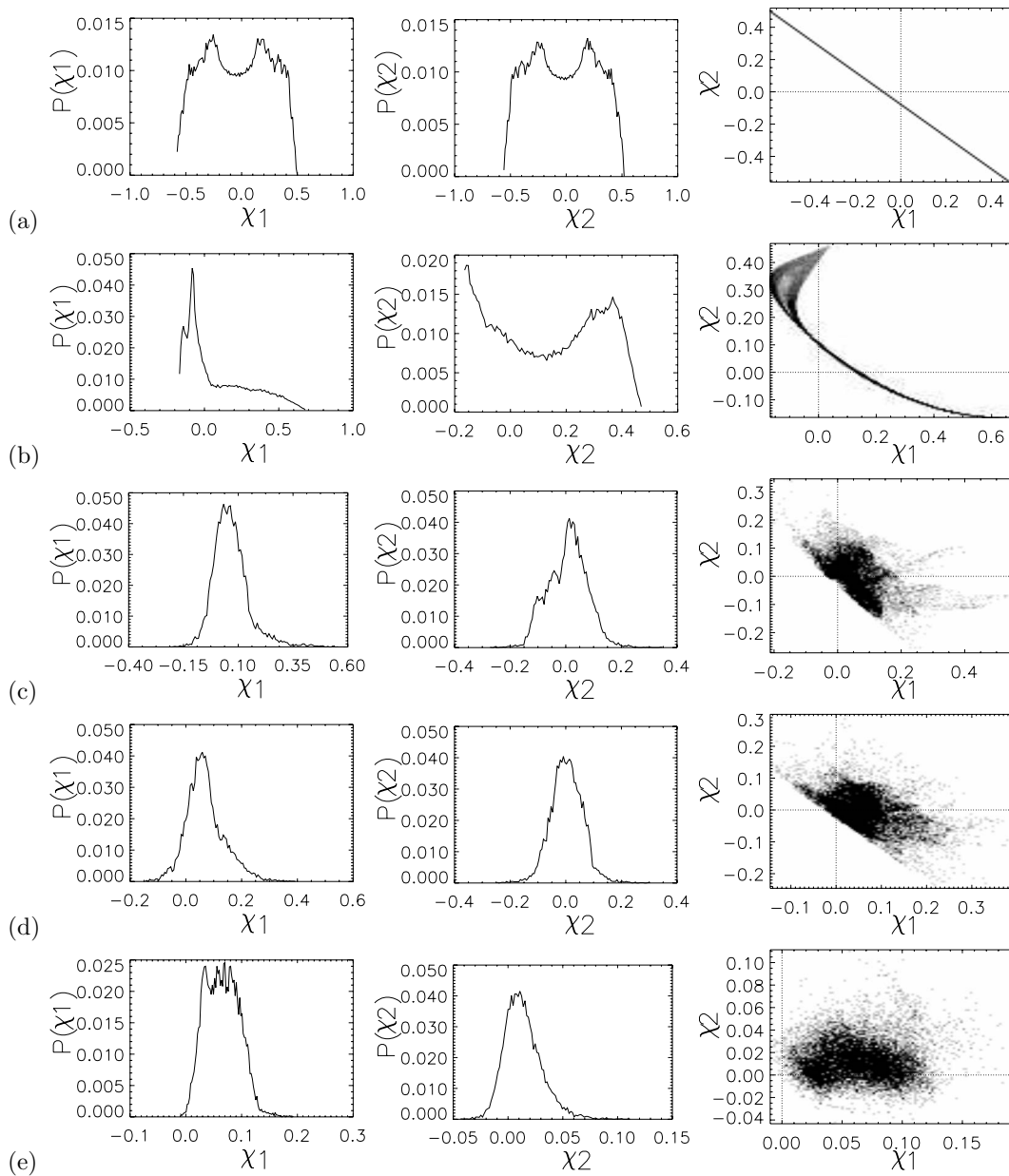


FIG. 4. Finite Lyapunov exponent distributions for the Eq. (3) Hamiltonian and  $\epsilon=4.6$ , chaotic orbit. (a)  $\Delta t=0.01$ , (b)  $\Delta t=1$ , (c)  $\Delta t=7$ , (d)  $\Delta t=10$ , (e)  $\Delta t=100$ .

odic orbit. However, in the tangent direction, the  $\chi_2$  distribution evolves at a different rate, and is still sign flipping.

Once again, as the time interval is larger than the given crossing time, for  $\Delta t=7$ , panel (c), the distributions are now different. When the interval is larger than  $T_{\text{cross}}$ ,  $\Delta t=10$ , panel (d), the distributions converge to the final measure, faster for  $\chi_1$ . With  $\Delta t=100$ , panel (e), both distributions resemble peaks centered in the asymptotic Lyapunov values  $\lambda_1 \sim 0.093$  and  $\lambda_2 \sim 0$ .

### C. Chaotic orbit, $\epsilon=4.6$

The Poincaré cross section appears in Fig. 1(c). The density functions for the first and the second Lyapunov exponents are plotted in Fig. 4. The numerical indexes which

characterize such distributions are found in Table III.

For the shortest intervals,  $\Delta t=0.01$ , panel (a), and  $\Delta t=0.1$ , not shown, both the  $\chi_1$  and  $\chi_2$  diagrams have widened and almost completely lost the two-peaks aspect from previous cases. For  $\Delta t=1$ , panel (b),  $\chi_1$  distribution changes in shape. With  $\Delta t=7$ , panel (c), both distributions are almost Gaussian. This is clearly observed with  $\Delta t=10$  and  $\Delta t=100$ , panels (d, e), centering around  $\lambda_1 \sim 0.066$  and  $\lambda_2$  values. Note however, that even when a Gaussian shape has been achieved quite fast at very short intervals, the peak of  $\chi_2$  is not still centered in the 0 value, implying a very low convergence of the averaging process.

This orbit is ergodic in the sense that the orbit is able to reach with the same probability all of its available phase space. It is interesting to keep in mind the difference between

TABLE III. Numerical indexes associated to the finite Lyapunov exponent distributions corresponding to Eq. (3), case  $\epsilon=4.6$ , chaotic orbit, for several  $\Delta t$  sizes. ( $\sigma$  is the standard deviation,  $k$  the kurtosis,  $F_+$  the probability of positivity,  $h$  the hyperbolicity index.)

$\Delta t$	Mean	Median	$\sigma$	k	$F_+$	$h$
			$\chi_1$			
0.01	-0.032	-0.031	0.29	-1.18	0.46	0.74
0.1	-0.041	-0.037	0.31	-1.14	0.46	0.84
1	0.091	-0.00092	0.22	-0.39	0.49	3.80
7	0.069	0.059	0.082	3.87	0.83	20.39
10	0.069	0.062	0.068	1.27	0.86	30.13
100	0.066	0.065	0.030	-0.19	0.99	142.49
			$\chi_2$			
0.01	-0.015	-0.017	0.29	-1.18	0.48	0.35
0.1	0.014	-0.0088	0.31	-1.14	0.50	0.28
1	0.13	0.15	0.19	-1.41	0.67	7.19
7	0.012	0.016	0.069	0.18	0.57	4.88
10	0.0067	0.0057	0.057	1.04	0.53	4.18
100	0.015	0.013	0.017	1.41	0.80	100.41

stationarity, due to the dynamics at a certain time, and ergodicity, time-averaged property of the trajectories. In a nonergodic orbit, the trajectory does not cover the whole hypersurface of constant energy, so two different initial conditions cover different parts of the energy surface leading to different temporal averages even for times tending to infinity. In such systems there is not a unique equilibrium state, but different ones depending on the starting point. In an ergodic system a unique equilibrium state may be reached. Generic ensembles of initial conditions will evolve towards a given distribution, time independent or with little variability on long time scales. In the case of conservative systems, there are no attractors and chaotic orbits are ergodic. But note that there may be the so-called sticky transients, where the orbits wander pseudochaotically with strictly zero Lyapunov exponent during some time around the KAM tori. Many authors refer then to such orbits as pseudoergodic ones. Such transients are the reason for the broad peaks found in the distributions.

## VI. FINITE LYAPUNOV EXPONENTS RELATIONSHIP

This section deals with the relationship between the largest finite exponent, associated to the transversal direction (if allowed to evolve), and second exponent, associated to the tangential one (id), when they are calculated by reinitializing arbitrarily the axes after an interval  $\Delta t$ .

Being large enough, the distribution of values will be driven uniquely by the transportation along the orbit, with no use on the linear equations of tangent space. When dealing with effective exponents (finite but large intervals), and for hyperbolic systems, there is a simple relationship between the first and second exponents, driven by the crowding indexes. For nonhyperbolic systems, the relationship may be more complicated [10]. Usually, there is multifractality, or

strong nontrivial dependence on the order  $q$  of the correlations [33]. We focus here on the relationship between exponents when computed for the smallest intervals where all multipliers (Lyapunov numbers) changing in sign contribute to the time decay and the correlations die very slow.

When comparing these distributions, it is needed to analyze if it is preserving the ordering of the exponents according to their magnitude. The definition given by Eq. (2) preserves the ordering as the axes evolve and a Gram-Schmidt orthonormalization takes place along  $\Delta t$ . But for the shortest intervals, there is not enough time for tending to the largest growth direction, and after resetting the direction of the ellipsoid axes, the locally largest exponent may or may not coincide with the previous annotated direction.

With this aim in mind, we have traced two-dimensional distribution histograms, of the second exponent against the first one. They conform the third box of every row in Figs. 2-4.

In the period-2,  $\epsilon=4.5$  case, and for the smallest intervals  $\Delta t=0.01$  and  $\Delta t=0.1$ , there is a linear relationship. When the local flow is expanding in one direction, it is contracting in the other one. Note a low probability region when both directions are contracting at time. For  $\Delta t=1$ , the correlation is no longer linear in the  $\chi_1$  contracting range. This is derived from a faster convergence rate towards the transversal direction. For the second exponent the distribution is still like a periodic one. When  $\Delta t$  increases, there is a clustering of the values towards the asymptotic values.

In the  $\epsilon=4.4$  case, the results are similar for  $\Delta t=0.01$  (panel a), and  $\Delta t=0.1$  (not shown), being the density plots also linear and below the origin. When the interval is larger,  $\Delta t=1$ , panel (b), we see a multivalued curve when there is expansion in the tangent direction. For  $\Delta t \sim T_{\text{cross}}$ , panel (c), the curve is now somehow more fuzzy. Now, the probability of finding both exponents expanding in time has increased. For  $\Delta t=10$ , panel (d) the points already cluster towards the asymptotic values.

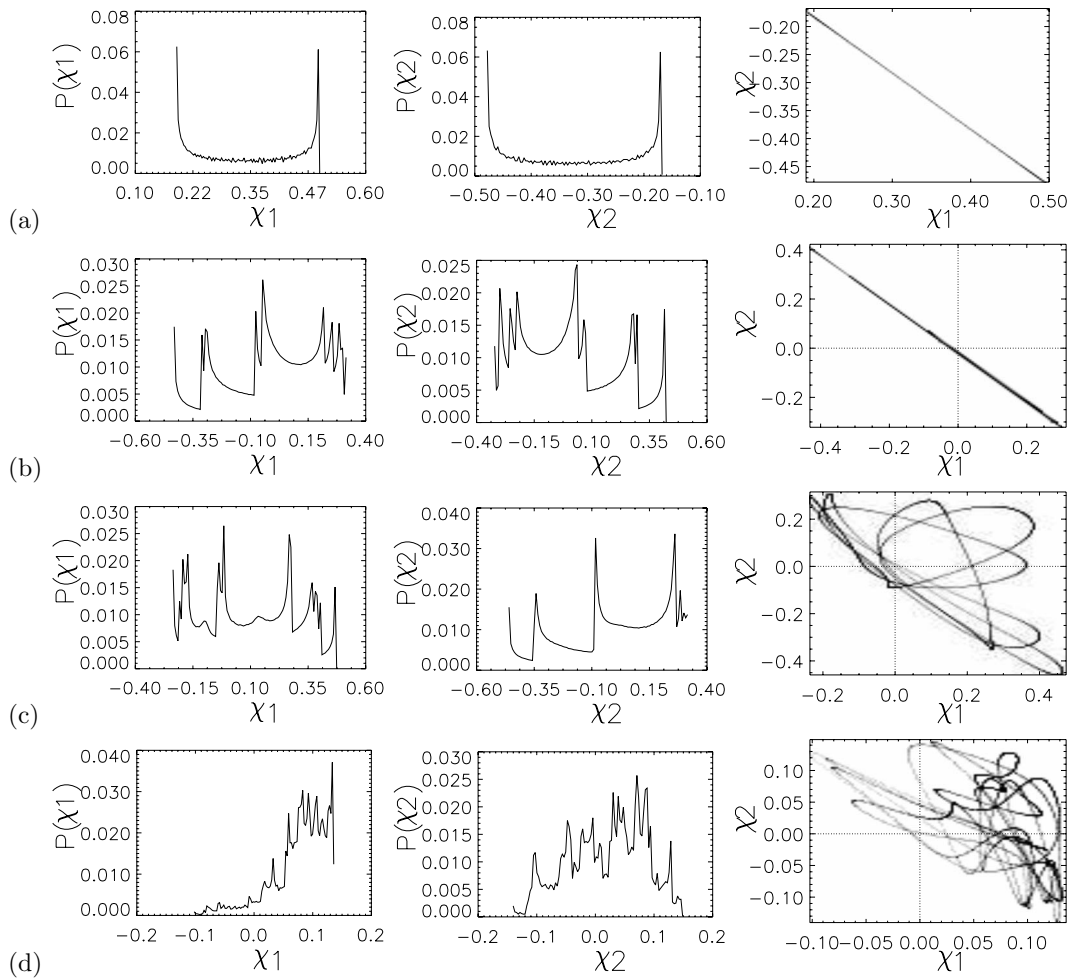


FIG. 5. Finite Lyapunov exponent distributions for the Hénon-Heiles Hamiltonian. (a) An unstable periodic orbit and  $\Delta t=0.01$ , (b) a period-5 orbit and  $\Delta t=0.01$ , (c) a period-5 orbit and  $\Delta t=1$ , (d) a period-5 orbit and  $\Delta t=10$ .

In the chaotic case,  $\epsilon=4.6$ , the relationship for the smaller intervals is also linear, and when expanding, the transversal direction contracts, and vice versa. When the finite time is increased up  $\Delta t \sim 1$ , the relationship curve in the expanding tangent direction part is more complicated. For  $\Delta t=7$  and  $\Delta t=10$  there is no correlation. For  $\Delta t=100$ , the curves converge to a set of points centered in the final values.

So the relationship is linear, independently of the nature of the orbit (periodic, confined between tori or chaotic) at the very local time scales, where no evolution towards any direction is allowed. This may be a direct consequence of the arbitrary starting direction for one axis and the orthogonality of the second. But this is the same for  $\Delta t=0.1$ , where many averaging steps have been performed and the vectors tend to seek the most rapidly growing directions. At these small intervals and after resetting the initial directions, the distributions still reflect the local nature of the flow, even when the finite values ordering could have been interleaved along the orbit. The comparison of the first and second distributions reflects that they essentially offer the same information.

In order to see if this holds for other systems, we have plotted in Figs. 5 and 6 the distributions and relationship diagrams for some prototypical orbits of the Hénon-Heiles system. The associated numerical indexes are found in Table

IV. In Fig. 5, panel (a), we see the plots at a very local scale  $\Delta t=0.01$  for another (unstable) periodic orbit with no oscillation around zero. The relationship diagram is also linear even when  $\chi_1$  is always expanding and  $\chi_2$  is always contracting. For a period-5 orbit, Fig. 5, panels (b), (c), and (d), a similar behavior is seen. Finally, in Fig. 6, we see the plots corresponding to a near (heteroclinic) cycle orbit. In this case, the complexity of the diagrams is similar to the ergodic case of the Eq. (3) model.

We conclude that the linear dependency at short intervals is related to the number of degrees of freedom of the system and the associated constraints in the Lyapunov values. Indeed, in Hamiltonian systems with more degrees of freedom this linear relationship is no longer present even for the smallest intervals.

## VII. NONHYPERBOLICITY, SHADOWING, AND PREDICTABILITY

In hyperbolic systems, the angle between the stable and unstable manifolds is away from zero and the phase space is locally spanned by a fixed number of distinct stable and unstable directions [34,35]. Nonhyperbolic behavior can arise from tangencies (homoclinic tangencies) between stable and

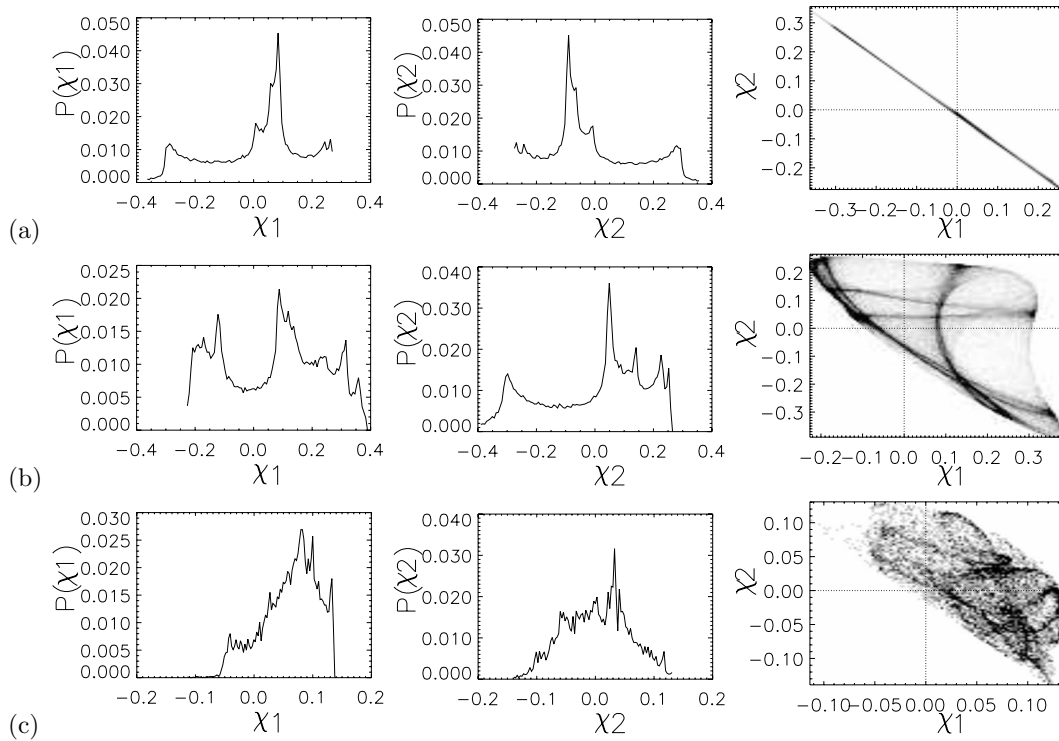


FIG. 6. Finite time Lyapunov exponent distributions for the Hénon-Heiles Hamiltonian. All panels are for the cycle orbit. (a)  $\Delta t=0.01$ , (b)  $\Delta t=1$ , (c)  $\Delta t=10$ .

unstable manifolds, from unstable dimension variability or from both. In the case of tangencies, there is a higher, but still moderate obstacle to shadowing. In the so-called pseudodeterministic systems, the shadowing is only valid during trajectories of reasonable length due to the unstable dimension variability (UDV).

The UDV is a property of the infinite number of UPO embedded in a chaotic invariant set, having a variation with position of the dimension of the invariant set subspaces (number of eigendirections). It was first reported in the kicked double rotor [36], where the invariant set of interest is a chaotic attractor. But UDV can also appear in nonattracting chaotic sets, which is our case. Several mechanisms lead to UDV, as bubbling transition in coupled oscillators, decoherence transitions in weakly coupled or nonidentical systems, hyperchaos or extrinsic noise, with associated intermittency [37–40]. Hyperchaos is a common source for UDV but is not possible in four-dimensional phase-space Hamiltonians.

In the selected model, both hyperbolic and nonhyperbolic behavior can be found. In the first case, all periodic orbits are unstable (only UPOs are found and chaotic saddles are the only invariant sets), without KAM tori. In the second, there are both UPO and KAM tori, KAM sticky orbits and chaotic sets. The UDV is reflected and quantified by the fluctuations around zero of the finite-time exponent closest to zero [41,42]. Fluctuations around zero of the maximum transient exponent were described for attractors of quasiperiodically forced systems in [43]. We must emphasize that there are situations where the positive tails appear not due to UDV but rather by other mechanisms, such as the quasitangencies between the stable and unstable manifolds near a homoclinic crisis point, for example. Such oscillations were detected by

both the largest and closest to zero exponents in analyzed Hamiltonians. This occurs both for  $\Delta t=0.01$  and  $\Delta t=0.1$ . Thus tending or not to the ellipse axes towards the largest stretching direction, the length scale for reflecting UDV seems to have the same threshold  $T_{\text{cross}}$  for both exponents, which are correlated and offer the same information. When increased the interval size, the distributions obtained from the closest to zero exponent have still  $F_+ \sim 0.5$ . This is no longer true for  $\chi_1$  distributions, which compress and finally lose the contracting side faster than  $\chi_2$ .

A key issue when there are strong obstacles to shadowing is the calculation of the shadowing time as a valid limit for the predictability of the system. This is especially relevant in high-dimensional systems, where it is hard to develop a good understanding of model accuracy or error growth. When the shadowing times are very short, averaged quantities as Lyapunov exponents may be handled with care, as the trajectories may suffer transient behaviors. This may lead to use finite exponents and “correct” shadowing times as averaging times. This is of special interest in Monte Carlo simulations, based on averaging results from many initial conditions [38].

The probability distributions for the shadowing can be justified from statistical properties of the finite-time exponents [37]. The shadowing time distributions with UDV present a scaling law algebraic for small shadowing times, and exponential for large ones (longer shadowing times are exponentially improbable). The shadowing distance typically increases exponentially when change in the unstable dimension occurs [44]. Then, it decreases exponentially in the hyperbolic regions, with a lower bound determined by the computer round-off. These switches occur randomly in time, so they mimic a (biased) random walk behavior, hence we can

TABLE IV. Numerical indexes associated to the finite Lyapunov exponent distributions corresponding to the Hénon-Heiles system, for one period-5 orbit and one unstable periodic orbit, and several  $\Delta t$  sizes. ( $\sigma$  is the standard deviation,  $k$  the kurtosis,  $F_+$  the probability of positivity,  $h$  the hyperbolicity index.)

$\Delta t$	Mean	Median	$\chi_1$ $\sigma$	k	$F_+$	$h$
UPO						
0.01	0.35	0.34	0.11	-1.50	1.00	56.53
Period-5						
0.01	0.0014	0.11	0.20	-0.90	0.51	0.0069
1	0.11	0.11	0.21	-1.22	0.62	5.13
10	0.077	0.086	0.047	1.52	0.92	70.93
Cycle						
0.01	0.0098	0.051	0.16	-0.70	0.62	0.78
1	0.074	0.098	0.17	-1.17	0.64	5.05
10	0.063	0.072	0.047	-0.31	0.87	56.37
$\Delta t$	Mean	Median	$\chi_2$ $\sigma$	k	$F_+$	$h$
UPO						
0.01	-0.32	-0.32	0.11	-1.50	0.00	52.39
Period-5						
0.01	0.0010	-0.0097	0.20	-0.90	0.48	0.0050
1	0.0053	0.028	0.22	-0.95	0.53	0.22
10	0.022	0.032	0.066	-0.81	0.61	10.15
Cycle						
0.01	-0.0092	-0.049	0.16	-0.70	0.36	0.74
1	0.00086	0.052	0.18	-0.99	0.60	0.054
10	0.0042	0.0053	0.054	-0.62	0.52	2.80

only give confidence to results where the amount of transversely attracting and repelling contributions nearly counterbalance (mean closest to zero) and expansions and contractions are well approximated by such a stochastic process.

The shadowing can also be described as a diffusion equation visualized as the interaction between holes, as escape routes along a given trajectory [45]. The effective range of the interactions is associated to the largest Lyapunov exponent. The shadowing is large when the holes are located in an unstable periodic orbit. The effects of the kicks in the pseudotrajectories are included as a reflecting barrier. Such diffusion process has an equilibrium distribution leading to a shadowing time  $\tau$  given by

$$\tau \sim \delta e^{-h}, \quad h = \frac{2\|m\|}{\sigma^2}. \quad (4)$$

The hyperbolicity exponent  $h$  depends on  $m$  and  $\sigma$ , the mean and the standard deviation of the Lyapunov exponent closest to zero, and on  $\delta$ , the round-off precision of the computer. The scaling laws for  $h$  are derived from the first and second cumulants [10,46]. The variance is inversely proportional to the interval in ergodic orbits [32], algebraic powers

are found when intermittency is present [29] or correlations decaying more slowly than the inverse of the time interval [47].

One important issue is to perform the  $h$  computation using a closest to zero exponent, since this exponent reflects in principle the varying number of unstable dimensions along the trajectory. We have calculated  $h$  both from the first and second indexes. The results are summarized in the tables and plotted in Fig. 7. In general,  $h$  grows with the interval length. For the shortest intervals, there are no Gaussian distributions and the values can not be regarded as random variables. The exponents oscillate and  $h$  keeps small, as the variance is small. For the non-UDV orbit of Henon-Heiles system,  $m$  is far from zero and  $h$  is large. When  $h$  computed from  $\chi_1$  is compared with that from  $\chi_2$ , the results are different even when both  $\chi_1$  and  $\chi_2$  fluctuate and are well correlated. The biased random walker model might not be fully applicable, but as the values are accumulated along a given orbit, they provide useful information in all orbit types, when computed from the second exponent  $h(\chi_2)$ .

For the largest intervals, distribution shapes are Gaussian-like, the correlations die out, and the ergodic theorem might be applied. The  $h(\chi_1)$  value has a wider span of values de-

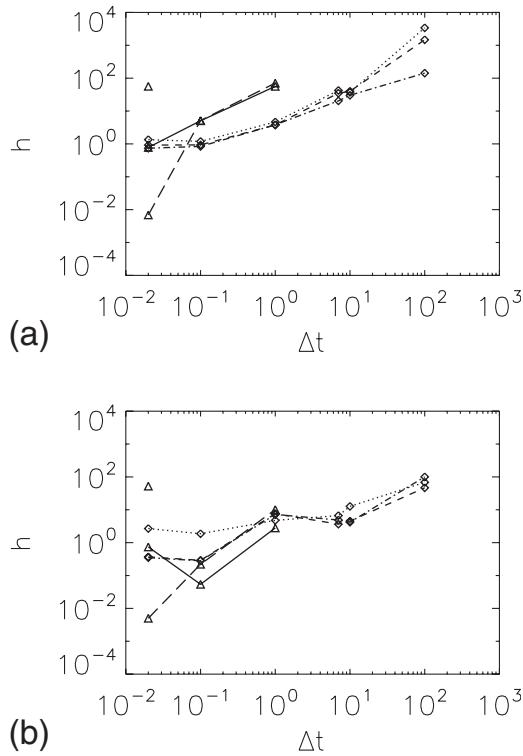


FIG. 7. Hyperbolicity index, calculated from the distributions of  $\chi_1$  (upper) and  $\chi_2$  (lower) finite-time Lyapunov exponents. Equation (3) Hamiltonian values are marked by diamonds, (dotted) period-2, (dashed) between tori orbit, (dashed dotted) chaotic. Hénon-Heiles Hamiltonian values are marked with triangles, (isolated point) UPO, (long dashed) period-5, (solid) cycle.

pending on the orbit type with the larger intervals, but  $h(\chi_2)$  has not.

### VIII. CONCLUSIONS

The results presented here are of a general interest in describing how the finite Lyapunov exponents and their distributions serve as valid indicators on the nature of a given orbit even when the initial axes have not been pointed to any specific direction. The knowledge of these ranges is of interest, because the finite exponents can be used for analyzing the local flow properties, such as plotting manifolds [48], or conversely, for tracing global properties, such as resonances, resonance overlap [6] or Arnold web [49].

We have seen that the information provided by the first and second exponents, seems to be the same when computed at very local scales. At larger intervals, but below a given threshold, when axes have been allowed to point to the larg-

est stretching direction, both exponents still trace the flow local properties, they oscillate around zero and may trace the UDV. At larger time scales, the linear relationship between both exponents is lost. We get global (averaged) values for the whole orbit or applicable domain of initial conditions, reaching the final asymptotic value at different rates. When both  $\chi_1$  and  $\chi_2$  are uncorrelated,  $\chi_1$ - $\chi_2$  diagrams may serve for tori identification or resonance mapping [50]. This is a quite interesting topic to extend the results of our work.

The linear relationship for the smallest intervals is of interest. This seems to be not orbit dependent, but due to the Hamiltonian system nature itself. For systems with larger number of degrees of freedom, this linear dependency is no longer true, even for the smallest intervals. Our work currently points in this direction, extending presented results to six-dimensional phase-space systems, where sticky transients are no longer present, cantori appears, and Arnold diffusion produce an ultimate merging of all orbits.

We have described how the hyperbolicity index varies when calculated from the largest and closest to zero exponents. They tend to the same value when the shapes are Gaussian-like and they are calculated from the closest to zero exponent. When calculated from the largest exponent, they depend on the orbit type.

At the shortest intervals, below the given threshold, the distributions are not Gaussian-like, and the random walker model is not valid. But both exponents detect UDV, and the values of  $h$  offer different predictability times for every orbit.

Finally, a key point to discuss is the physical meaning of the involved integration times. We must balance carefully a physically meaningful time scale with a reliable computation time, pointed by the shadowing index. For instance, the number of dynamical times relevant in Hamiltonian systems usually found in galactic dynamics and plasma physics, are rather different. If the physical time scales for obtaining the global properties are too long for being realistic, the characterization derived from selected ensembles will not be able to be used as a valid skeleton for the observed system behavior. Conversely, if we want to analyze just the local properties, it is important to keep in mind the maximum time scale to trace it.

### ACKNOWLEDGMENTS

This work was supported by the Spanish Ministry of Science and Technology under Contract No. BFM2003-03081, by the Spanish Ministry of Education and Science under Contract No. FIS2006-08525, and by Universidad Rey Juan Carlos and Comunidad de Madrid under Contract No. URJC-CM-2006-CET-0643.

[1] G. M. Zaslavsky, R. Z. Sagdeev, D. A. Usikov, and A. A. Chernikov, *Weak Chaos and Quasi-Regular Patterns* (Cambridge University Press, Cambridge 1991).  
 [2] H. Flaschka, *Phys. Rev. B* **9**, 1924 (1974).

[3] N. Voglis, G. Contopoulos, and C. Efthymiopoulos, *Celest. Mech. Dyn. Astron.* **73**, 211 (1999).  
 [4] Ch. Skokos, *J. Phys. A* **34**, 10029 (2001).  
 [5] P. M. Cincotta and C. Simo, *Astron. Astrophys.* **147**, 205

- (2000).
- [6] C. Froeschle and E. Lega, *Celest. Mech. Dyn. Astron.* **78**, 167 (2000).
- [7] J. Tailleur and J. Kurchan, *Nat. Phys.* **3**, 203 (2007).
- [8] G. Boffetta, M. Cencini, M. Falcioni, and A. Vulpiani, *Phys. Rep.* **356**, 367 (2002).
- [9] R. Badii, K. Heinzlmann, P. F. Meier, and A. Politi, *Phys. Rev. A* **37**, 1323 (1988).
- [10] P. Grassberger, R. Badii, and A. Politi, *J. Stat. Phys.* **51**, 135 (1988).
- [11] T. Kapitaniak, *Phys. Rev. E* **47**, 1408 (1993).
- [12] C. Ziehmann, L. A. Smith, and J. Kurths, *Phys. Lett. A* **271**, 237 (2000).
- [13] K. Ramasubramanian and M. S. Sriram, *Physica D* **139**, 72 (2000).
- [14] G. Benettin, L. Galgani, and J. M. Strelcyn, *Phys. Rev. A* **14**, 2338 (1976).
- [15] R. Doerner, B. Hubinger, W. Martienssen, S. Grossmann, and S. Thoma, *Chaos, Solitons Fractals* **10**, 1759 (1999).
- [16] B. Joseph and B. Legras, *J. Atmos. Sci.* **59**, 1198 (2002).
- [17] N. Voglis, G. Contopoulos, and C. Efthymiopoulos, *Phys. Rev. E* **57**, 372 (1998).
- [18] Ch. Vozikis, H. Varvoglis, and K. Tsiganis, *Astron. Astrophys.* **359**, 386 (2000).
- [19] A. Crisanti, G. Paladin, and A. Vulpiani, *Product of Random Matrices*, Springer Series in Solid State Sciences (Springer, Berlin, 1993).
- [20] C. Anteneodo, *Phys. Rev. E* **69**, 016207 (2004).
- [21] J. C. Vallejo, J. Aguirre, and M. A. F. Sanjuan, *Phys. Lett. A* **311**, 26 (2003).
- [22] G. Contopoulos, *Astron. J.* **75**, 96 (1970).
- [23] J. Binney and S. Tremaine, *Galactic Dynamics* (Princeton University Press, Princeton, NJ, 1987).
- [24] G. Contopoulos, E. Grousousakou, and N. Voglis, *Astron. Astrophys.* **304**, 374 (1995).
- [25] W. I. Newman and A. Y. Lee, *Bull. Am. Astron. Soc.* **37**, 531 (2005).
- [26] T. J. Stuchi, *Braz. J. Phys.* **32**, 4 (2002).
- [27] G. Parisi and A. Vulpiani, *J. Phys. A* **19**, L425 (1986).
- [28] J. D. Meiss, *Physica D* **74**, 254 (1994).
- [29] A. Prasad and R. Ramaswamy, *Phys. Rev. E* **60**, 2761 (1999).
- [30] J. D. Szezech, Jr., S. R. Lopes, and R. L. Viana, *Phys. Lett. A* **335**, 394 (2005).
- [31] L. A. Smith and E. A. Spiegel, in *Chaotic Phenomena in Astrophysics*, edited by J. R. Buchler and H. Eichhorn (New York Academy of Sciences, New York, 1987).
- [32] T. Kottos, A. Politi, F. M. Izrailev, and S. Ruffo, *Phys. Rev. E* **53**, R5553 (1996).
- [33] P. Grassberger, *Phys. Lett.* **107A**, 101 (1985).
- [34] R. L. Viana and C. Grebogi, *Phys. Rev. E* **62**, 462 (2000).
- [35] H. Kantz, C. Grebogi, A. Prasad, Y. C. Lai, and E. Sinde, *Phys. Rev. E* **65**, 026209 (2002).
- [36] R. Abraham and S. Smale, *Proc. Symp. Pure Math.* **14**, 5 (1970).
- [37] R. L. Viana, S. E. Pinto, J. R. Barbosa, and C. Grebogi, *Int. J. Bifurcation Chaos Appl. Sci. Eng.* **11**, 1 (2003).
- [38] T. D. Sauer, *Phys. Rev. E* **65**, 036220 (2002).
- [39] T. D. Sauer, *Chaos* **13**, 947 (2003).
- [40] E. Barreto and P. So, *Phys. Rev. Lett.* **85**, 2490 (2000).
- [41] R. L. Davidchack and Y. C. Lai, *Phys. Lett. A* **270**, 308 (2000).
- [42] R. L. Viana, J. R. Barbosa, C. Grebogi, and C. M. Batista, *Braz. J. Phys.* **35**, 1 (2005).
- [43] T. Kapitaniak, *Prog. Theor. Phys.* **93**, 831 (1995).
- [44] Y. Do and Y. C. Lai, *Phys. Rev. E* **69**, 016213 (2004).
- [45] H. Buljan and V. Paar, *Phys. Rev. E* **63**, 066205 (2001).
- [46] M. A. Sepulveda, R. Badii, and E. Pollak, *Phys. Rev. Lett.* **63**, 1226 (1989).
- [47] S. Tomsovic and A. Lakshminarayan, *Phys. Rev. E* **76**, 036207 (2007).
- [48] M. Valluri and D. Merrit, *Astrophys. J.* **506**, 686 (1998).
- [49] S. Honjo and K. Kaneko, e-print arXiv:nlin.CD/0307050v1.
- [50] J. von Milczewski, G. H. F. Diercksen, and T. Uzer, *Phys. Rev. Lett.* **76**, 2890 (1996).